

Article

Two Birds with One Stone: Preparation of 4,4-Diaminodiphenylmethane Functionalized GO@SiO₂ with Mechanical Reinforcement and UV Shielding Properties and Its Application in Thermoplastic Polyurethane

Guoxin Ding ^{1,*} , Hongxu Tai ¹, Chuanxin Chen ¹, Chenfeng Sun ¹ and Zhongfeng Tang ^{2,*}

¹ School of Materials Science and Engineering, Anhui University of Science and Technology, Huainan 232001, China; thx0315@163.com (H.T.); CCX0720@foxmail.com (C.C.); The_Shadower@163.com (C.S.)

² Shanghai Institute of Applied Physics, Chinese Academy of Sciences, Shanghai 201800, China

* Correspondence: dgx480@163.com (G.D.); tangzhongfeng@sinap.ac.cn (Z.T.)

Abstract: This study prepared 4,4-diaminodiphenylmethane (DDM)-functionalized graphene oxide (GO)@silica dioxide (SiO₂) nano-composites through amidation reaction and low-temperature precipitation. The resulting modified GO, that was DDM-GO@SiO₂. The study found that DDM-GO@SiO₂ showed good dispersion and compatibility with thermoplastic polyurethane (TPU) substrates. Compared with pure TPU, the tensile strength of the TPU composites increased by 41% to 94.6 MPa at only 0.5 wt% DDM-GO@SiO₂. In addition, even when a small amount of DDM-GO@SiO₂ was added, the UV absorption of TPU composites increased significantly, TPU composites can achieve a UV shielding efficiency of 95.21% in the UV-A region. These results show that this type of material holds great promise for the preparation of functional coatings and film materials with high strength and weather resistance.

Keywords: graphene oxide; silicon dioxide; mechanical properties; thermoplastic polyurethane; ultraviolet



Citation: Ding, G.; Tai, H.; Chen, C.; Sun, C.; Tang, Z. Two Birds with One Stone: Preparation of 4,4-Diaminodiphenylmethane Functionalized GO@SiO₂ with Mechanical Reinforcement and UV Shielding Properties and Its Application in Thermoplastic Polyurethane. *Polymers* **2021**, *13*, 4220. <https://doi.org/10.3390/polym13234220>

Academic Editors: Tao-Hsing Chen and Shih-Chen Shi

Received: 14 November 2021

Accepted: 26 November 2021

Published: 1 December 2021

Publisher's Note: MDPI stays neutral with regard to jurisdictional claims in published maps and institutional affiliations.



Copyright: © 2021 by the authors. Licensee MDPI, Basel, Switzerland. This article is an open access article distributed under the terms and conditions of the Creative Commons Attribution (CC BY) license (<https://creativecommons.org/licenses/by/4.0/>).

1. Introduction

Thermoplastic polyurethane (TPU) is a multi-segment copolymer consisting of hard and soft segments [1]. It is also an important elastomeric polymer. Given its abundant sources and good processing properties, TPU is widely used in packaging materials, functional coatings, and other applications [2–4]. However, the applications of TPU are limited by its low mechanical strength and poor weather resistance [5–7]. In addition, TPU is prone to automatic oxidation and yellowing under UV light, making this polymer brittle and yellow [8,9]. Thus, many functional materials have been used to prepare TPU-based composites [10,11]. Two-dimensional carbon materials, particularly graphene oxide (GO), have been widely used for the production of high-performance polymers because of their unique mechanical and optical properties [12,13]. The key issues in GO/polymer nanocomposites are how to address dispersion and interfacial forces [14]. Chemical modification is an effective way of solving both problems [15–17]. Ren et al. [18] used ethylenediamine to prepare cross-linked GO and found that ethylenediamine filled into TPU improves the dispersion of GO while significantly increasing the tensile strength and elongation at break. Halima et al. [19] used acetamide-modified GO, which is homogeneously dispersed into PU as a filler, to improve the anti-corrosion properties of PU. The dispersion of GO in polymers can also be improved by modifying it with nanomaterials [20]. The in situ growth of silica (SiO₂) on the surface of GO improves dispersion and reduces interfacial forces; meanwhile, the modification of SiO₂ imparts a highly porous surface structure to GO, which provides non-covalent attachment points and improves the physical entanglement between GO and TPU [21]. Kim et al. [22] attached nano-SiO₂ onto the surface of GO

by using the sol-gel method and found that silica modification enhances the polarity of the surface, which generates a chemical affinity between the SiO₂/GO nanocomposite and TPU. Yu et al. [21] obtained graphene/SiO₂ composites by in situ preparation and introduced the hybrid nanoparticles into epoxy resins. They found that the unique 3D structure of graphene/SiO₂ increases the interfacial adhesion between the filler and the matrix and significantly improves the mechanical properties of the epoxy resins. SiO₂/GO nanocomposites not only improve the mechanical properties of the polymer but also protect against UV light. The conjugated groups and aromatic structures on the surface of GO provide good absorption of UV light [23], whereas those of SiO₂ can reflect UV light [24] and can be added to polymers to act as a barrier and reduce damage caused by UV light to the polymer matrix.

This study proposed a simple and environment-friendly method. DDM-GO@SiO₂ nanocomposites were obtained by the hydrophobic modification of GO using 4,4-diaminodiphenylmethane (DDM) and in situ chemical growth of SiO₂ nanocomposites on DDM-GO by using potassium silicate water glass. DDM-GO@SiO₂ was dispersed into TPU by solution blending. DDM-GO@SiO₂ was successfully characterized using scanning electron microscopy (SEM), infrared (IR) spectroscopy, X-ray diffraction (XRD), Raman spectroscopy, X-ray photoelectron spectroscopy (XPS), and other methods. The effects of different additions of DDM-GO@SiO₂ on the mechanical properties and UV shielding properties of TPU were also focused on.

2. Materials and Methods

2.1. Materials

GO was supplied by Tan Feng Tech., Inc, Jiangsu, China. DDM, ammonium hydroxide, *N,N*-dimethylformamide (DMF), ethyl alcohol, and sodium dodecyl benzene sulfonate (SDBS) were obtained from Sinopharm Chemical Reagent Co., Ltd., Shanghai, China. Hydrochloric acid with an HCl content of 37.5% was purchased from Jia Ni Chemical Co., Ltd., Jiangsu, China. These reagents are of analytical grade. TPU (WHT-1195) was acquired from Wan Hua Chemical Group Co., Ltd., Hubei, China. Potassium silicate was supplied by Usolf Chemical Tech., Inc, Shandong, China. Deionized water was homemade and then used for all experimental procedures.

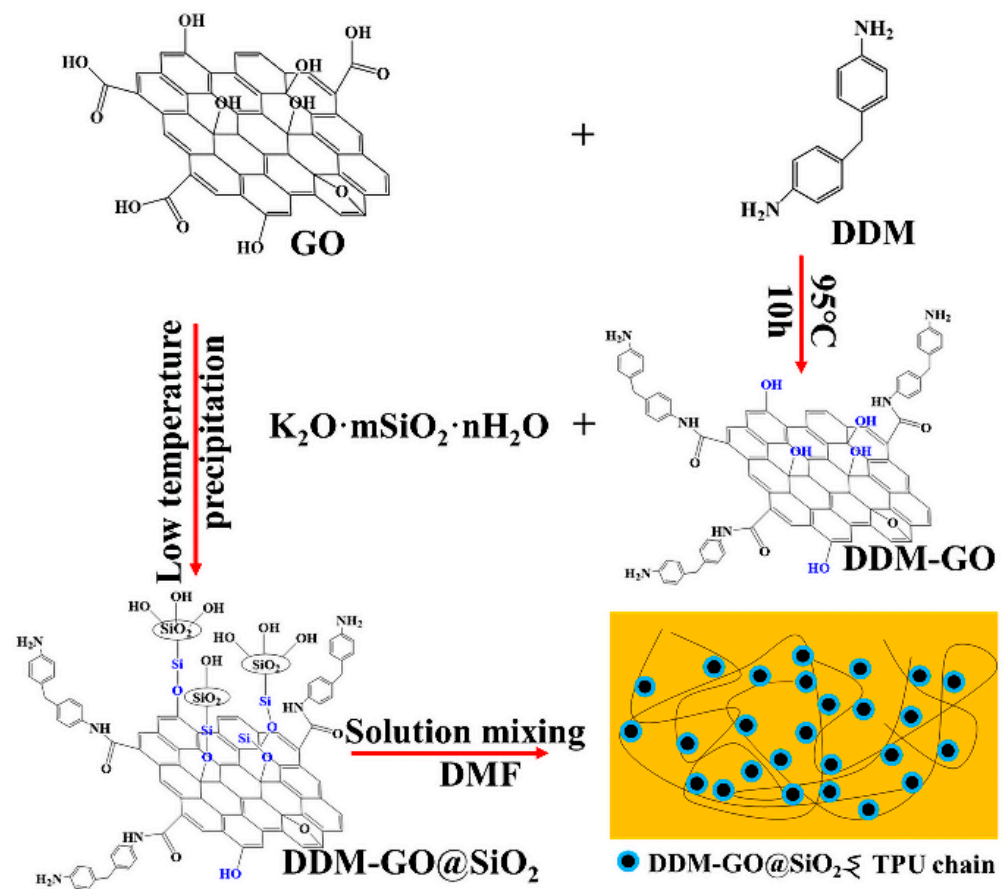
2.2. Preparation of DDM-GO@SiO₂ Particle

1.5 g of DDM was added at 95 °C to 300 mL of deionised water sonicated with 0.5 g of GO. The mixture was magnetically stirred at 95 °C for 10 h and then DDM-GO was obtained by vacuum filtration of the mixture several times using deionized water and freeze-dried.

3.0 g potassium silicate was added to 50 mL of deionised water sonicated with 0.5 g DDM-GO and 0.2 g SDBS. The pH of the mixture was adjusted to 7 by hydrochloric acid in an ice water bath and maintained for 12 h. Lastly, DDM-GO@SiO₂ composites were obtained by vacuum filtration of the mixture several times using deionized water and freeze-dried.

2.3. Preparation of the DDM-GO@SiO₂/TPU Composites

DDM-GO@SiO₂ composites were added to 100 mL of DMF, ultrasonically dispersed for 20 min, and then heated to 80 °C. TPU (10.0 g) was dissolved into the dispersion, stirred at high speed for 4 h, placed in a mold, and de-bubbled in a vacuum drying oven at 80 °C. Then, the DMF was dried out to prepare DDM-GO@SiO₂/TPU composites. DDM-GO@SiO₂ nanocomposites were filled with 0, 0.1, 0.3, 0.5, 1, and 2 wt% of the total TPU and denoted as S0, S1, S2, S3, S4, and S5, respectively. Scheme 1 showed the preparation procedure of DDM-GO@SiO₂/TPU composites.



Scheme 1. Preparation procedure of DDM-GO@SiO₂/TPU composites.

2.4. Characterization

Characteristic peaks of the material were analyzed via Fourier-transform infrared (FT-IR) spectroscopy (AVATAR370, Thermo Nicolet, MA, USA). The crystal structure of the material was characterized using XRD (Smartlab SE, Japanese Science, Tokyo, Japan) with a scanning diffraction angle of 5°–80° and a step size of 5°/min. The chemical composition of the material was determined with XPS (ESCALAB 250Xi, Thermo Fischer, MA, USA). Bond and structural defects of the material were analyzed using Raman spectroscopy (In Via, Renishaw, Gloucestershire, UK) at a wavelength of 532 nm. The microstructure of the material was examined via SEM (Gemini 300, ZEISS, Oberkochen, Germany) operating at 10 kV, and local elemental analysis was performed via energy dispersive spectroscopy (EDS, Xplore, Oxford, UK) at 20 kV. Cross-sectional scanning of the TPU composites was brittle broke in liquid nitrogen. The specimens were subjected to tensile tests using GB/T 528-2009. The testing apparatus was a universal testing machine (WDW-50, Kaiqiagli Testing Apparatus Co., Ltd., Shenzhen, China). Absorbance and transmittance of the materials were tested on a UV-VIS-NIR spectrophotometer (Lambda950, PerkinElmer, MA, USA).

3. Results and Discussion

3.1. DDM-GO@SiO₂ Particles Structure

Figure 1a displayed the FT-IR spectra of GO, DDM-GO, and DDM-GO@SiO₂ particles. The FT-IR spectrum of GO demonstrates O–H vibration, C=O vibration, C=C stretching vibration, C–H vibration, and C–O stretching vibration peaks at 3406, 1723, 1626, 2923, and 1069 cm^{−1}, respectively [25]. The FT-IR spectrum of DDM-GO shows that the peak at 1038 cm^{−1} is the stretching vibration of C–N [26]. The decrease in intensity of the absorption peak associated with the carboxyl group is due to a decrease in the number of oxygen-containing groups on the GO surface. Amination reaction result in the red shift of

C=O at $1723\text{--}1630\text{ cm}^{-1}$ because of $p\text{--}\pi$ conjugation [27]. These results indicate that GO is successfully reduced via DDM. As shown in Figure 1b, the Si–OH and Si–O–Si peaks of DDM–GO@SiO₂ at 800 and 477 cm^{-1} , respectively, are consistent with the characteristic peaks of SiO₂ [28]. The Si–O–C stretching vibration peak appears at 1054 cm^{-1} , and O–H presents a lower peak intensity compared with DDM–GO possibly because of the reaction of the hydroxyl group on the surface of DDM–GO with Si–OH on the surface of SiO₂ to generate Si–O–C via dehydration [29]. Hence, the reduction of the hydroxyl group on the surface of DDM–GO indicates the successful grafting of SiO₂ on the surface of DDM–GO.

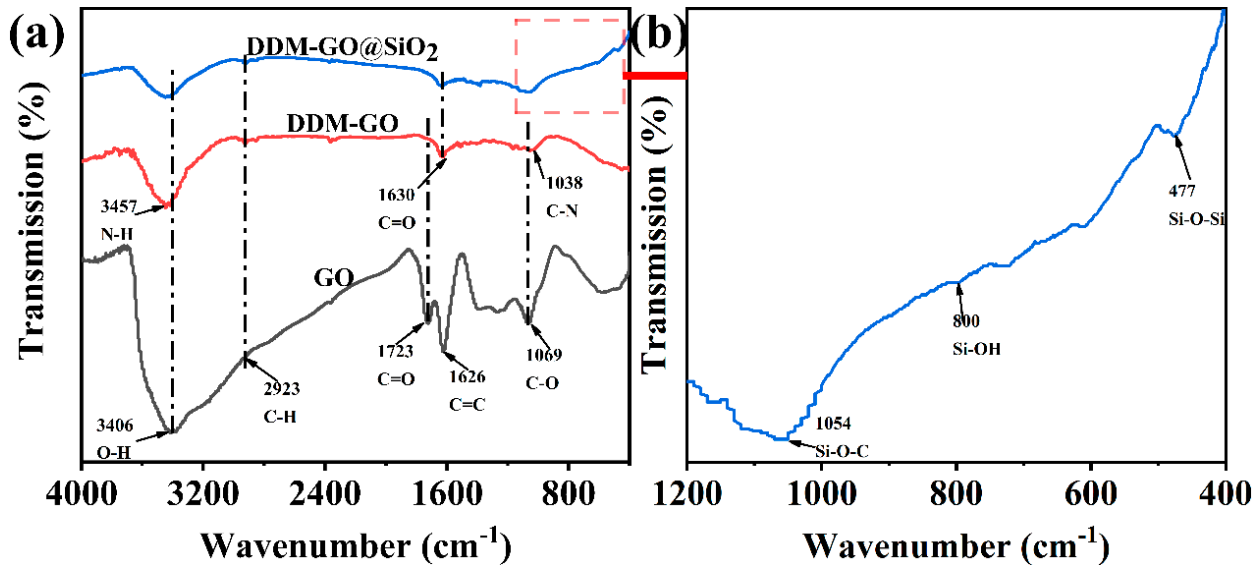


Figure 1. (a) FT–IR spectra of GO, DDM–GO, DDM–GO@SiO₂, (b) partial enlarged view of DDM–GO@SiO₂.

XPS tests were performed on DDM–GO@SiO₂ to assess whether or not the modification was successful. The total XPS spectrum of DDM–GO@SiO₂ in Figure 2a presents characteristic peaks corresponding to Si2p, C1s, N1s, and O1s. N element is derived from the modifier DDM, and Si element is derived from the SiO₂ graft on the DDM–GO surface. Figure 2b shows the presence of N element in three forms. Fitted peaks of N1s at 398.6, 399.2, and 399.8 eV correspond to Pyridinic N, Pyrrolic N, and Graphitic N [30]. As shown in Figure 2c, fitted peaks at 104.2, 104.5, and 105.3 eV for Si2p correspond to Si–O–C, Si–O–Si, and Si–OH, respectively [31]. As shown in Figure 2d, fitted peaks at 284.1, 284.9, 286.1, 290.7 and for C1s correspond to C–OH, C–N, C–COOH and C*, respectively [32].

XRD spectra of GO, DDM–GO and DDM–GO@SiO₂ were illustrated in Figure 3a. GO presents two diffraction peaks at $2\theta = 11.7^\circ$ and 42.5° , which correspond to (001) and (100) crystal planes [33]. The comparison of XRD spectra of DDM–GO and GO show that the (001) crystalline plane disappears and a new diffraction peak appears at $2\theta = 20.1^\circ$, indicating the successful reduction of GO [34]. The XRD spectrum of DDM–GO@SiO₂ shows a broad peak at $2\theta = 22.7^\circ$, which corresponding to the (111) crystal plane of SiO₂ nanoparticles. This result suggests that the SiO₂ particles cover the layered GO sheets successfully.

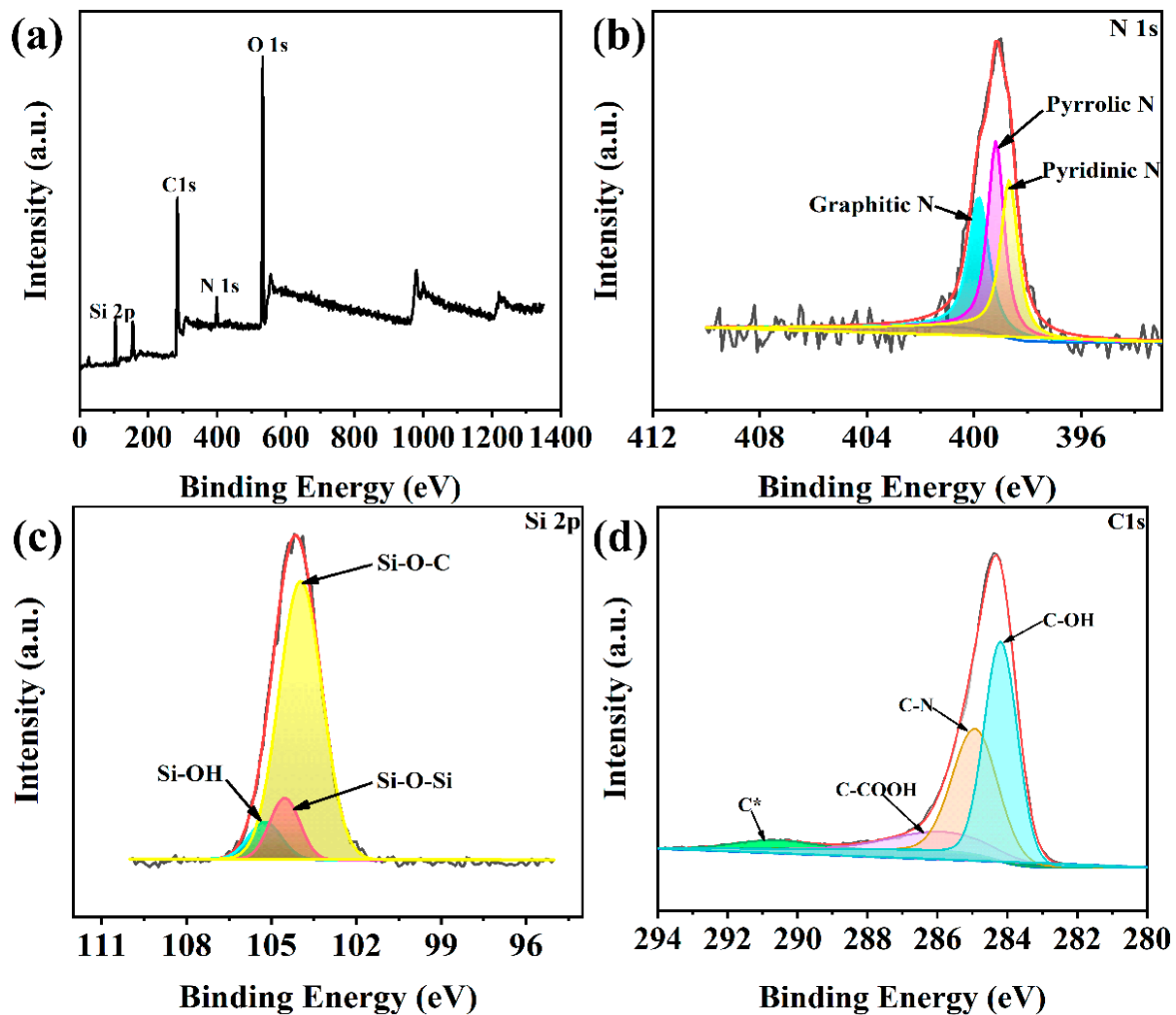


Figure 2. XPS spectra of DDM-GO@SiO₂ composites (a) Survey XPS spectra, (b) N1s, (c) Si 2p, (d) C1s.

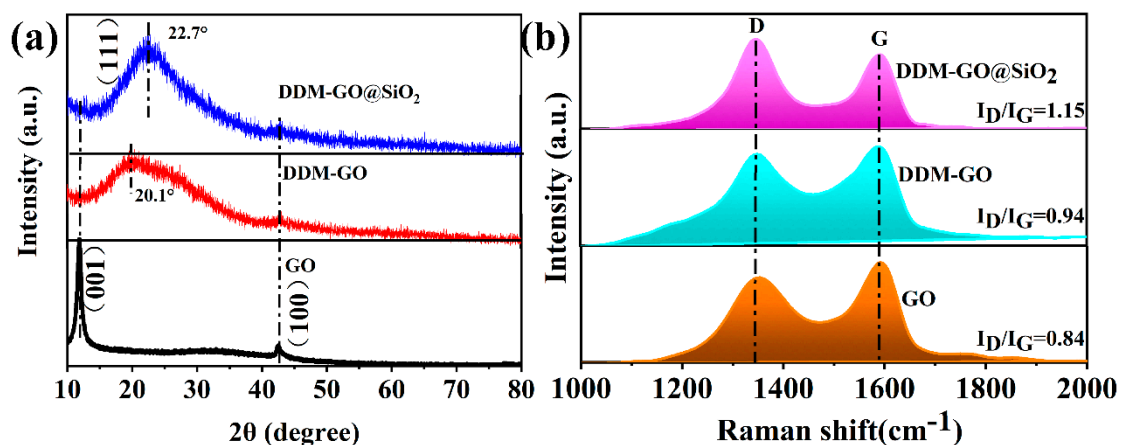


Figure 3. (a) XRD spectra of GO, DDM-GO, DDM-GO@SiO₂, (b) Raman spectra GO, DDM-GO, DDM-GO@SiO₂.

Raman spectra of GO, DDM-GO, and DDM-GO@SiO₂ show two distinctive peaks attributed to the G and D bands. The G band, which represents the E_{2g} vibrational mode of first-order scattering and is used to characterize the sp² bond structure of carbon, appeared at 1591 cm⁻¹. The D band, which is a reflection of the disorder of the crystalline structure, appeared at 1347 cm⁻¹ [35]. The ratio of D band/G band (I_D/I_G) intensity is an indicator of the extent of surface defects in carbon materials. The increment in D peak intensity implies

the broken sp^2 bonds and the presence of more sp^3 bonds on the sheets. As shown in Figure 3b, the I_D/I_G ratio was calculated to be 0.84 for GO, 0.94 for DDM–GO, and 1.15 for DDM–GO@SiO₂. The higher I_D/I_G value of DDM–GO than GO is due to the reaction of DDM with oxygen-containing groups on the GO surface, resulting in more surface defects after GO deoxidation. Meanwhile, the higher I_D/I_G value of DDM–GO@SiO₂ than DDM–GO indicates the increased disorder caused by the grafting of SiO₂ onto DDM–GO. The results are similar to the study of Kou [36].

Microscopic morphologies of GO, DDM–GO, and DDM–GO@SiO₂ were analyzed through SEM. Figure 4a,b show the smooth surface of GO sheet and the wrinkles on the reduced DDM–GO sheet. DDM as a reducing agent destroys the hexagonal carbon backbone of GO, introducing defects and loss of long-range ordering on the surface of the graphene sheet, causing it to wrinkle [37]. As shown in Figure 4c, the surface of DDM–GO@SiO₂ is rougher than that of DDM–GO with many attached SiO₂ particles. By contrast, the morphology of DDM–GO@SiO₂ is similar to that of GO modified with a tetraethylsilicate mixture [38]. The EDS mapping analysis in Figure 4d is used to confirm the distribution of SiO₂ on DDM–GO. Successful modification of GO by DDM was further demonstrated due to the presence of N element. It can be seen that Si element is evenly distributed in the system, which shows that SiO₂ is well dispersed in DDM–GO.

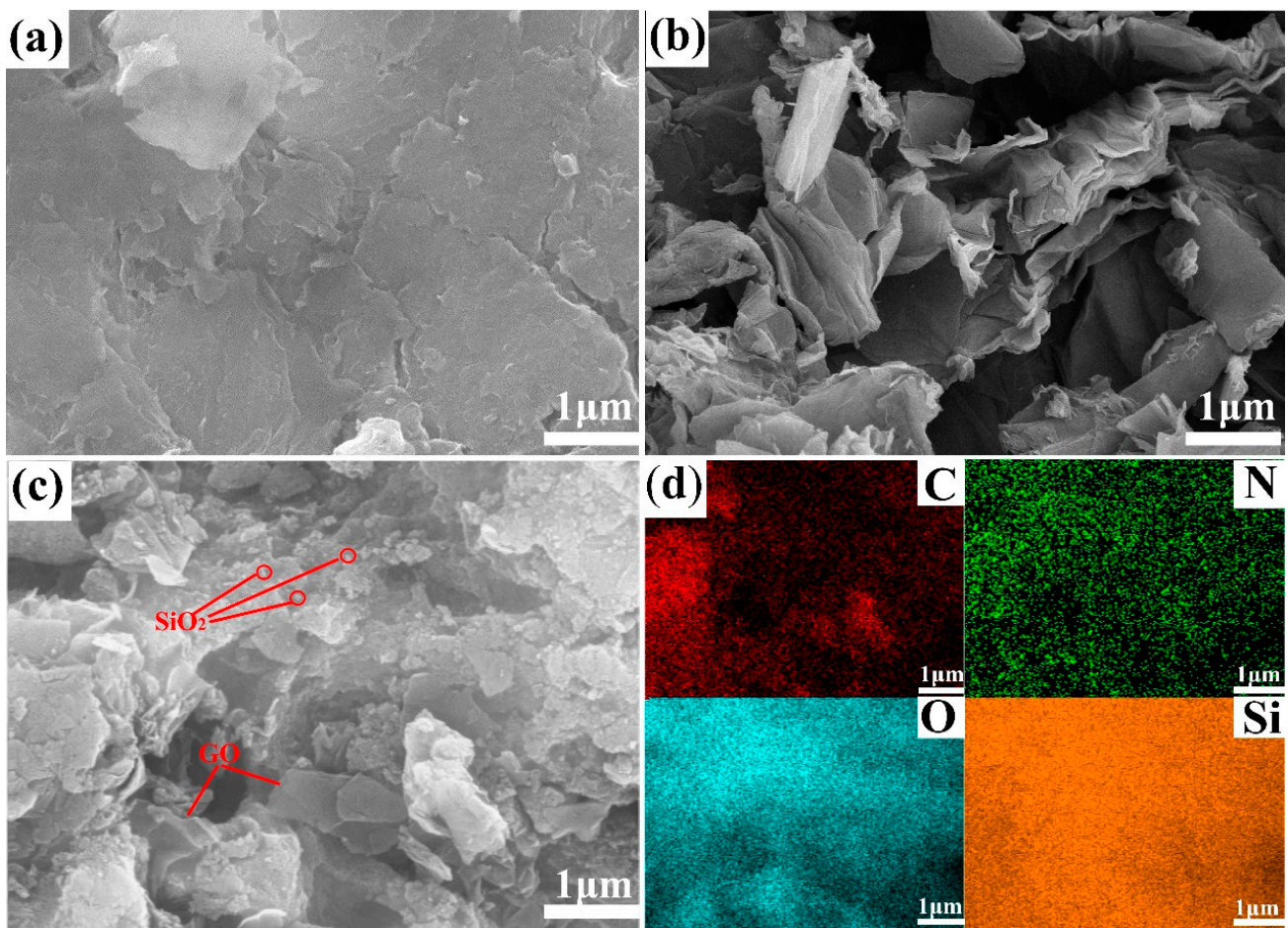


Figure 4. SEM image of (a) GO, (b) DDM–GO, (c) DDM–GO@SiO₂; (d) EDS mapping spectra of DDM–GO@SiO₂.

3.2. Mechanical and UV-Shielding Performance Analysis

The stress–strain analysis was used to investigate the mechanical properties of TPU and the effect of DDM–GO@SiO₂ content on the mechanical properties of the nanocomposites. Stress–strain curves and the corresponding tensile strength and elongation at break

of the TPU composites with different DDM–GO@SiO₂ fillings were shown in Figure 5a,b. Compared with that of pure TPU, the tensile strength of the TPU composites with 0.5 wt% DDM–GO@SiO₂ filling content increased by 41% to 94.6 MPa. The significant increase in tensile strength can be attributed to the increased forces between DDM–GO@SiO₂ and TPU. However, the tensile strength of the nanocomposites gradually decreased as the content of DDM–GO@SiO₂ exceeded 0.5 wt%. The elongation at break also decreased with increasing DDM–GO@SiO₂ content. This phenomenon can be explained by the fact that the degree of deformation of the TPU molecular chains is limited at high DDM–GO@SiO₂ loadings, leading to a reduction in the strain at break. Furthermore, a high amount of DDM–GO@SiO₂ may lead to aggregation in the TPU matrix and induce the formation of defects, leading to a decline in mechanical properties [39]. The stretching vibration peak of N–H in the TPU matrix is very sensitive to changes in hydrogen bonding. Therefore, the hydrogen bonding changes between DDM–GO@SiO₂ and TPU were characterised by FT-IR tests. As shown in Figure 5c, with the addition of DDM–GO@SiO₂, the N–H stretching vibration peak of the TPU composite blue shifts from 3331 cm⁻¹ to 3333 cm⁻¹, which is attributed to the addition of the filler breaking the hydrogen bond within the TPU and forming a stronger hydrogen bond between the filler and TPU matrix. The hydrogen bond between DDM–GO@SiO₂ and TPU is shown schematically in Figure 5f. However, when the filler content is further increased, the peak is red shifted, which is attributed to agglomeration of filler affecting the formation of hydrogen bonds. In addition, as shown in Figure 5d, the stretching vibration peaks at 1732 cm⁻¹ and 1703 cm⁻¹ correspond to “free” C=O and bonded C=O in TPU, respectively. For every N–H bond created between DDM–GO@SiO₂ and TPU, a new “free” C=O is formed [40]. A Gaussian fit is made to the curve in Figure 5d to investigate the variation in C=O. As shown in Figure 5e, the free C=O peak area/C=O peak area values of the TPU composites are higher than pure TPU [41,42], indicating a strong interaction between DDM–GO@SiO₂ and TPU, the trend also corresponds to the change in mechanical properties.

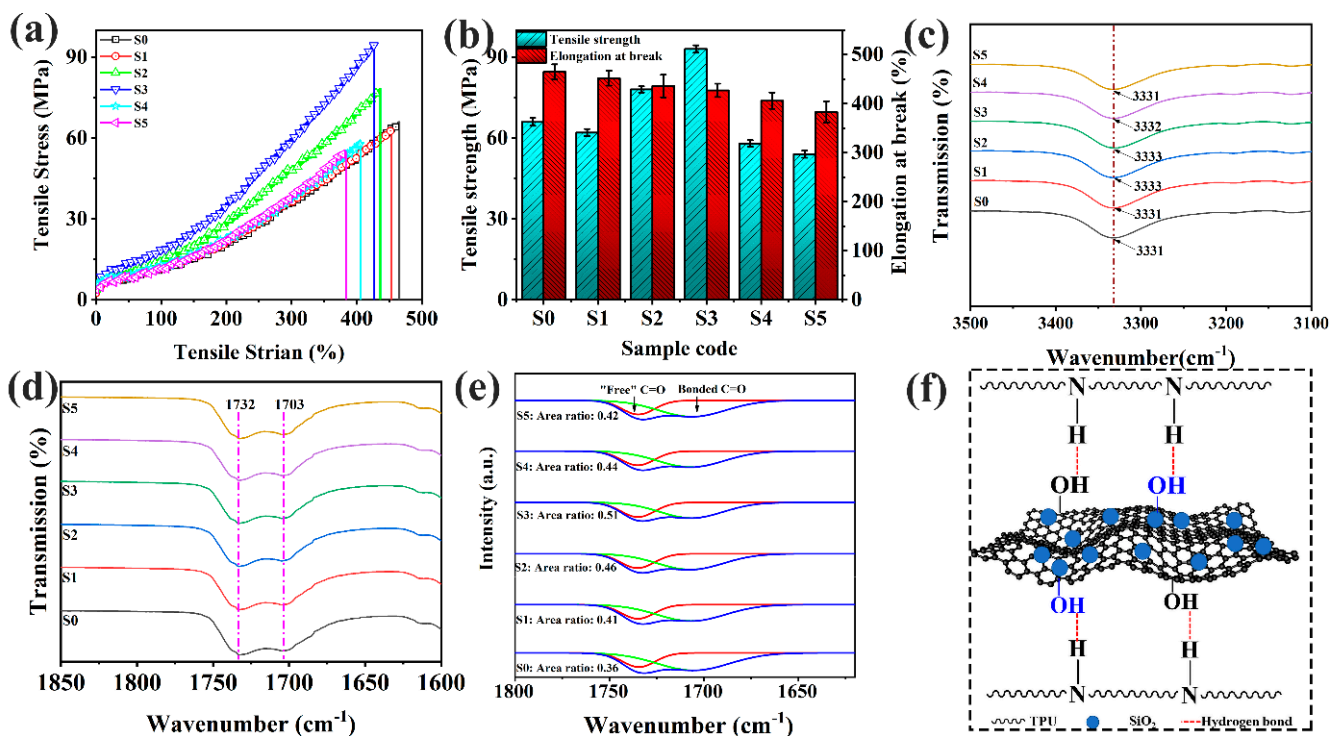


Figure 5. Mechanical properties of TPU nanocomposites: (a) stress–strain curves and (b) statistical results of tensile strength and elongation at break; FT-IR spectra of TPU composites at the range of (c) 3500 cm⁻¹–3100 cm⁻¹, (d) 1850 cm⁻¹–1600 cm⁻¹, (e) curve fitting diagram of the carbonyl stretching region (f) schematic diagram of the microstructure of TPU composites.

The transmittance and absorbance spectra of samples, including pure TPU and TPU nanocomposites with different DDM–GO@SiO₂ contents from 0.1 wt% to 2 wt%, were obtained to analyze the UV-shielding performance of the DDM–GO@SiO₂/TPU nanocomposites over the entire UV range. Figure 6a, b showed the absorbance and transmittance spectra of the samples in the wavelength range of 200–800 nm. The strong and wide UV absorption band at 321 nm is observed in pure TPU, accredited as n-π* leap absorption peak from C=O [43]. The UV absorption band at 233 nm is observed in the TPU composites, accredited as π-π* leap absorption peak from C=C. Notably, the C=O absorption peak of the TPU nanocomposite appears at 339 nm, showing a significant red shift along with greater absorption because of the enhanced interaction of DDM–GO@SiO₂ and TPU [44]. The absorption peak of SiO₂ is observed at a peak of 380 nm. The introduction of DDM–GO@SiO₂ increases the absorbance of TPU within the entire UV region (200–400 nm), and the absorbance increases gradually with increasing content. As shown in Figure 6b, the transmittance of the TPU composites is reduced compared with that of pure TPU, especially in the UV-A and UV-B regions, where the transmittance decreases significantly with increasing DDM–GO@SiO₂ content. This result is due to the reflection of UV light by SiO₂ and the strong absorption of incident UV light by the GO sheet layer, thus protecting the internal structure of TPU. The relevant schematic is shown in Figure 6d. The blocking efficiency in the UV-A and B regions is summarized in Table 1 to quantify the UV shielding property of the DDM–GO@SiO₂/TPU nanocomposites. The blocking efficiency at given UV ranges can be calculated using the following equations [45]:

$$\text{UV-A blocking (\%)} = 100 - \frac{\int_{320}^{400} T(\lambda)d\lambda}{\int_{320}^{400} d\lambda} \quad (1)$$

$$\text{UV-B blocking (\%)} = 100 - \frac{\int_{280}^{320} T(\lambda)d\lambda}{\int_{280}^{320} d\lambda} \quad (2)$$

As shown in Figure 6c, the addition of DDM–GO@SiO₂ improves the UV shielding efficiency in the UV-A and UV-B regions, especially in the UV-A region, which is the most serious for TPU UV aging. When the content of DDM–GO@SiO₂ is 2 wt%, the shielding efficiency can reach 95.21% from 79.25% of pure TPU. The specific data are shown in Table 1.

Table 1. Blocking efficiencies of samples in the UV-A and B regions.

Sample	Blocking Efficiency (%)	
	UV-B (280–320 nm)	UV-A (320–400 nm)
S0	83.21	79.25
S1	91.92	92.35
S2	92.28	93.53
S3	92.47	94.02
S4	92.48	94.65
S5	92.52	95.21

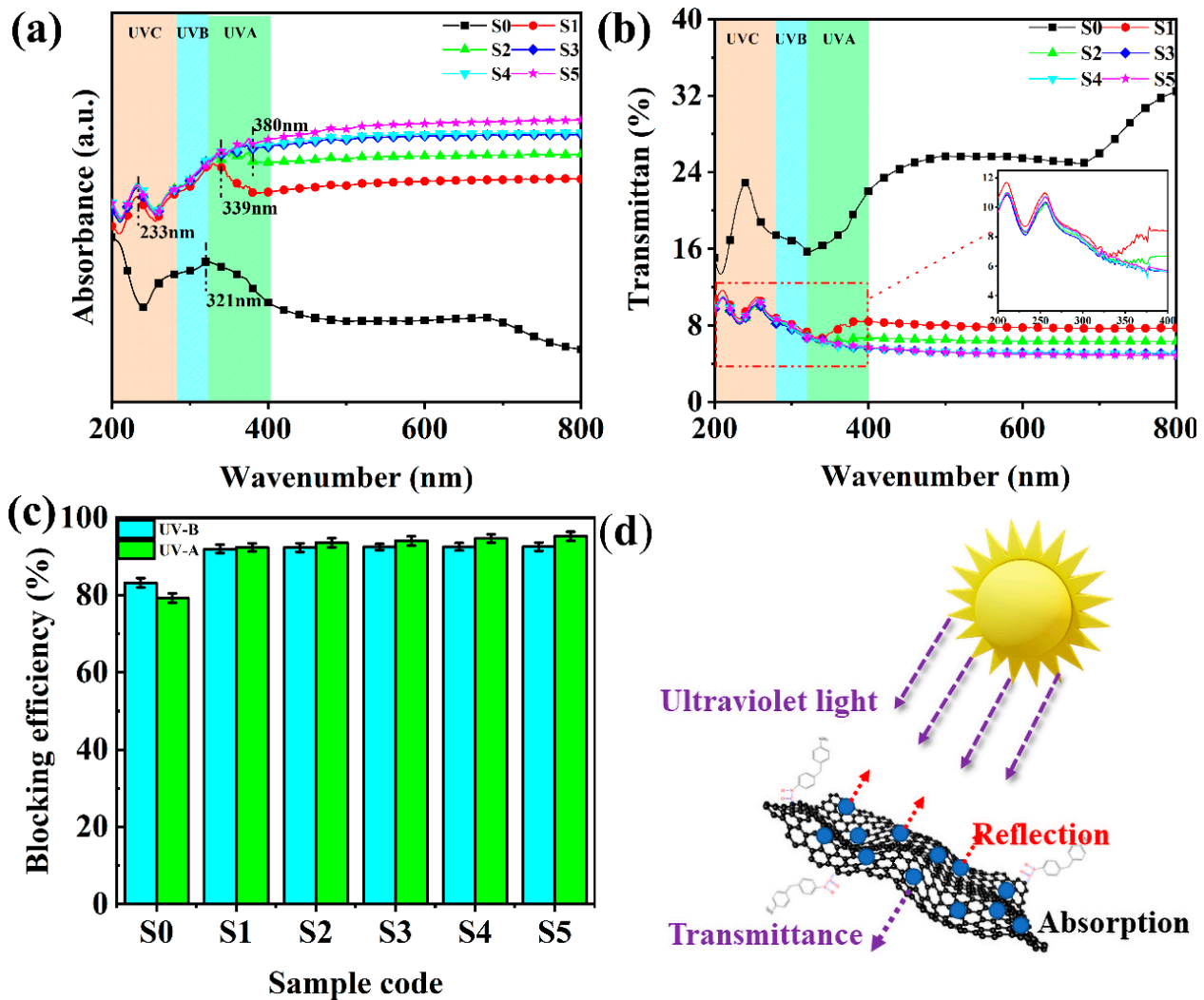


Figure 6. (a) Absorbance, (b) Transmittance, (c) UV shielding performance comparison of TPU composites, (d) Diagram of the shielding effect of DDM-GO@SiO₂ against UV light.

3.3. Cross-Sectional Morphology of TPU Composites Analysis

The cross-sectional morphology of the polymer was characterized using SEM to investigate the dispersion and interfacial interaction of DDM-GO@SiO₂ in TPU. Wavy and relatively smooth cross-sectional morphology is observed in pure TPU, as shown in Figure 7a. Similar fracture surfaces are also observed in the TPU composites (Figure 7b–f). In addition, the roughness at the fracture interface of the TPU composite become richer, which may be caused by crack bridging and pull-out DDM-GO@SiO₂. As the loading of DDM-GO@SiO₂ increased above 1 wt%, significant agglomeration and cracks occur in the cross section of the TPU composites (Figure 7e,f). Many cavities and agglomerates appear on the fracture surface with the increase in DDM-GO@SiO₂ filling because of the agglomeration of the filler in TPU and the decrease in the interfacial bonding force. It is completely pulled out during the tensile process. The higher magnification SEM image and EDS spectra of the circular area of the 0.5 wt% DDM-GO@SiO₂/TPU composite are shown in Figure 7g,h. The presence of Si and N elements can be clearly detected by EDS [46].

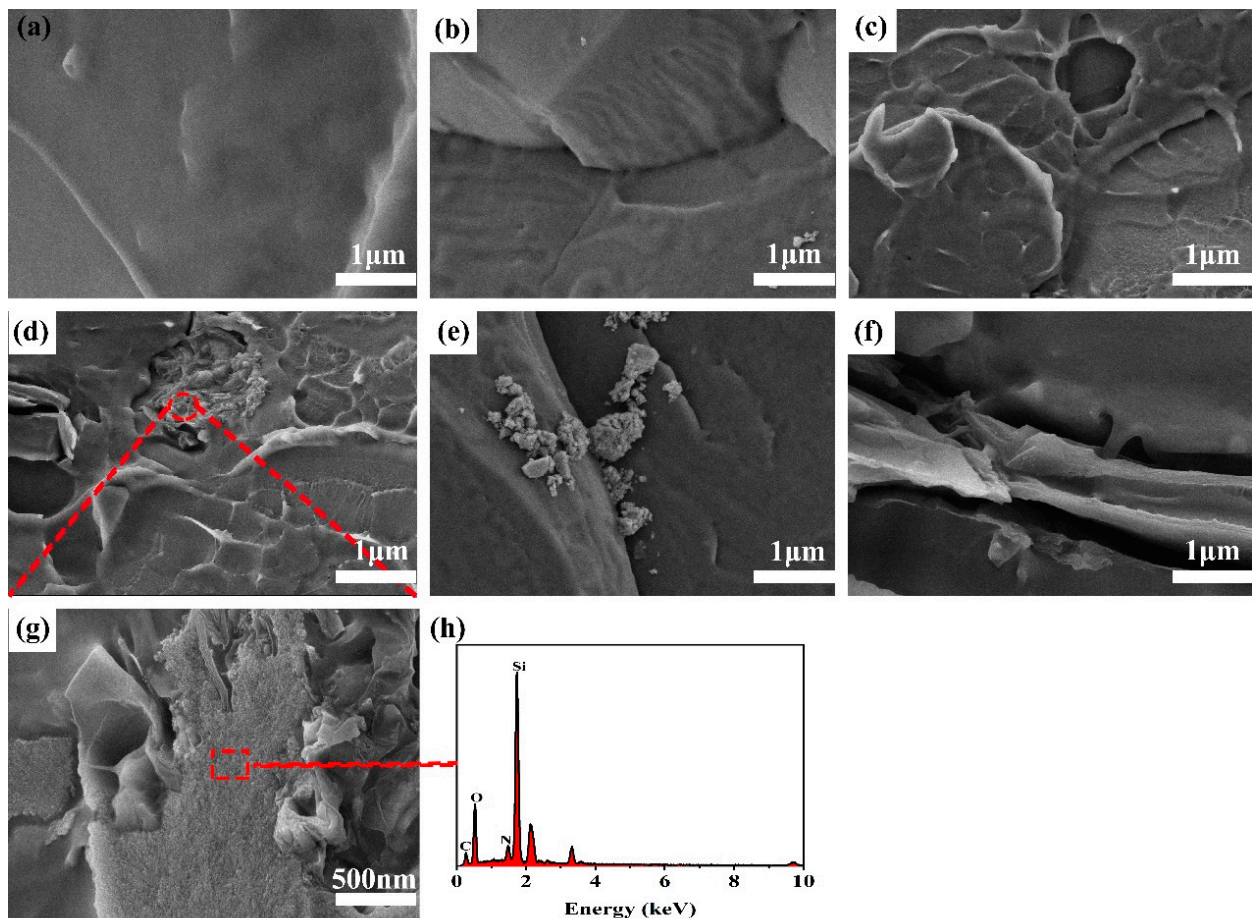


Figure 7. Cross-sectional SEM of TPU composites with different fillings (a) S0 (b) S1 (c) S2 (d) S3 (e) S4 (f) S5, (g) enlarged view of the red circle (h) EDS spectra of the red circle.

4. Conclusions

In this work, DDM was used to hydrophobically modify GO to improve dispersion in TPU. DDM–GO@SiO₂ nanocomposites were obtained by depositing nano-SiO₂ on the surface of DDM–GO by in situ growth. The introduction of nano-SiO₂ provides non-covalent attachment points and further improves DDM–GO physical entanglement with TPU. Meanwhile, DDM–GO and SiO₂ have a synergistic effect in reinforcing and shielding UV light. TPU composites with different DDM–GO@SiO₂ contents were prepared by solution blending. Compared with that of pure TPU, the tensile strength of the TPU composites with a filling amount of 0.5 wt% increased by 41%, reaching 94.6 MPa. Benefiting from the absorption of UV light by GO and reflection by SiO₂, in the UV-A region, when the DDM–GO@SiO₂ content is only 2 wt%, the transmission rate is significantly reduced, and its shielding efficiency can reach 95.21% from 79.25% of pure TPU. In addition, the DDM–GO@SiO₂/TPU composites have the advantages of a simple preparation process and low cost. This type of material holds great promise for functional coatings and high-performance thin film materials.

Author Contributions: G.D.: Methodology, Conceptualization, Formal analysis, Resources, Writing—review & editing. H.T.: Data curation, Writing—original draft, Software. C.C.: Writing—review & editing, Data curation. C.S.: Writing—review & editing, Data curation. Z.T.: Writing—review & editing, Resources. All authors have read and agreed to the published version of the manuscript.

Funding: This research was funded by the National Key R&D Program of China (2018YFB1501002), the Key Technologies R&D Program of Anhui Province of China (202104a05020033), Anhui University

of Science and Technology Introduced Talent Research Startup Fund (13190203), Huainan Science and Technology Project (2021A241).

Institutional Review Board Statement: Not applicable.

Informed Consent Statement: Not applicable.

Data Availability Statement: This study did not report any data.

Conflicts of Interest: The authors declare no conflict of interest.

References

1. Wang, X.L.; Wang, L.B.; He, Y.; Wu, M.; Zhou, A.G. The effect of two-dimensional d-Ti₃C₂ on the mechanical and thermal conductivity properties of thermoplastic polyurethane composites. *Polym. Compos.* **2019**, *41*, 350–359. [[CrossRef](#)]
2. Li, X.Y.; Wang, G.L.; Yang, C.X.; Zhao, J.C.; Zhang, A.M. Mechanical and EMI shielding properties of solid and microcellular TPU/nanographite composite membranes. *Polym. Test.* **2021**, *93*, 106891. [[CrossRef](#)]
3. Wang, X.; Liu, X.H.; Schubert, D.W. Highly Sensitive Ultrathin Flexible Thermoplastic Polyurethane/Carbon Black Fibrous Film Strain Sensor with Adjustable Scaffold Networks. *Nano-Micro Lett.* **2021**, *13*, 1–19. [[CrossRef](#)]
4. Lin, L.W.; Choi, Y.J.; Chen, T.Y.; Kim, H.; Lee, K.S.; Kang, J.; Lyu, L.; Gao, J.F.; Piao, Y.Z. Superhydrophobic and wearable TPU based nanofiber strain sensor with outstanding sensitivity for high-quality body motion monitoring. *Chem. Eng. J.* **2021**, *419*, 129513. [[CrossRef](#)]
5. Bailly, M.; Kontopoulou, M.; el Mabrouk, K. Effect of polymer/filler interactions on the structure and rheological properties of ethylene-octene copolymer/nanosilica composites. *Polymer* **2010**, *51*, 5506–5515. [[CrossRef](#)]
6. Ma, X.; Zhang, M. Preparation and Properties of Graphene Oxide-Modified Anti-UV Waterborne Polyurethane Nanocomposites. *Nano* **2020**, *15*, 2050005. [[CrossRef](#)]
7. Zou, W.K.; Dong, J.T.; Luo, Y.W.; Zhao, Q.; Xie, T. Dynamic Covalent Polymer Networks: From Old Chemistry to Modern Day Innovations. *Adv. Mater.* **2017**, *29*, 1606100. [[CrossRef](#)]
8. Das, S.; Pandey, P.; Mohanty, S.; Nayak, S.K. Investigation into the Influence of UV Aging on Green Polyurethane/Nanosilica Composite Coatings Based on Transesterified Castor Oil and Palm Oil Isocyanate. *J. Inorg. Organomet. Polym. Mater.* **2017**, *27*, 641–657. [[CrossRef](#)]
9. Yang, L.; Lu, X.L.; Wang, Z.H.; Xia, H.S. Diels–Alder dynamic crosslinked polyurethane/polydopamine composites with NIR triggered self-healing function. *Polym. Chem.* **2018**, *9*, 2166–2172. [[CrossRef](#)]
10. Pourmohammadi-Mahunaki, M.; Haddadi-Asl, V.; Roghani-Mamaqani, H.; Koosha, M.; Yazdi, M. Halloysite-reinforced thermoplastic polyurethane nanocomposites: Physico-mechanical, rheological, and thermal investigations. *Polym. Compos.* **2020**, *41*, 3260–3270. [[CrossRef](#)]
11. Cui, Z.X.; Lin, J.X.; Zhan, C.H.; Wu, J.H.; Shen, S.; Si, J.H.; Wang, Q.T. Biomimetic composite scaffolds based on surface modification of polydopamine on ultrasonication induced cellulose nanofibrils (CNF) adsorbing onto electrospun thermoplastic polyurethane (TPU) nanofibers. *J. Biomater. Sci. Polym. Ed.* **2020**, *31*, 561–577. [[CrossRef](#)]
12. Wang, Y.; Liu, X.Y.; Xu, X.; Yang, Y.; Huang, L.H.; He, Z.Y.; Xu, Y.H.; Chen, J.J.; Feng, Z.S. Preparation and characterization of reduced graphene oxide/Fe₃O₄ nanocomposite by a facile in-situ deposition method for glucose biosensor applications. *Mater. Res. Bull.* **2018**, *101*, 340–346. [[CrossRef](#)]
13. Naeimi, A.; Amini, M.; Okati, N. Removal of heavy metals from wastewaters using an effective and natural bionanopolymer based on Schiff base chitosan/graphene oxide. *Int. J. Environ. Sci. Technol.* **2021**, 1–12. [[CrossRef](#)]
14. Ramanathan, T.; Abdala, A.A.; Stankovich, S.; Dikin, D.A.; Herrera-Alonso, M.; Piner, R.D.; Adamson, D.H.; Schniepp, H.C.; Chen, X.; Ruoff, R.S.; et al. Functionalized graphene sheets for polymer nanocomposites. *Nat. Nanotechnol.* **2008**, *3*, 327–331. [[CrossRef](#)]
15. Wu, C.; Huang, X.Y.; Wang, G.L.; Wu, X.F.; Yang, K.; Li, S.T.; Jiang, P.K. Hyperbranched-polymer functionalization of graphene sheets for enhanced mechanical and dielectric properties of polyurethane composites. *J. Mater. Chem.* **2012**, *22*, 7010–7019. [[CrossRef](#)]
16. Zhang, Y.; Mark, J.E.; Zhu, Y.; Ruoff, R.S.; Schaefer, D.W. Mechanical properties of polybutadiene reinforced with octadecylamine modified graphene oxide. *Polymer* **2014**, *55*, 5389–5395. [[CrossRef](#)]
17. Zhang, Y.; Mark, J.E.; Zhu, Y.W.; Ruoff, R.S.; Schaefer, D.W. Simultaneous surface functionalization and reduction of graphene oxide with octadecylamine for electrically conductive polystyrene composites. *Carbon* **2011**, *49*, 4724–4730.
18. Ren, H.; Zhou, Y.M.; He, M.; Xu, R.; Ding, B.B.; Zhong, X.; Tong, Y.; Fan, L.D.; Cai, Z.L.; Shen, H.; et al. Enhanced mechanical properties of silica nanoparticle-covered cross-linking graphene oxide filled thermoplastic polyurethane composite. *New J. Chem.* **2018**, *42*, 3069–3077. [[CrossRef](#)]
19. Khatoun, H.; Iqbal, S.; Ahmad, S. Covalently functionalized ethylene diamine modified graphene oxide poly-paraphenylene diamine dispersed polyurethane anticorrosive nanocomposite coatings. *Prog. Org. Coat.* **2021**, *150*, 105966. [[CrossRef](#)]
20. Chen, Z.X.; Lu, H.B. Constructing sacrificial bonds and hidden lengths for ductile graphene/polyurethane elastomers with improved strength and toughness. *J. Mater. Chem.* **2012**, *22*, 12479–12490. [[CrossRef](#)]

21. Yu, K.J.; Wang, M.L.; Qian, K.; Lu, X.F.; Sun, J. The synergy effect of Graphene/SiO₂ hybrid materials on reinforcing and toughening epoxy resin. *Fibers Polym.* **2017**, *17*, 453–459. [[CrossRef](#)]
22. Kim, H.W.; Yoon, J.H.; Diederichsen, K.M.; Shin, J.E.; Yoo, B.M.; McCloskey, B.D.; Park, H.B. Exceptionally Reinforced Polymer Nanocomposites via Incorporated Surface Porosity on Graphene Oxide Sheets. *Macromol. Mater. Eng.* **2017**, *302*, 1700039. [[CrossRef](#)]
23. Duan, L.; Zhang, T.; Song, W.H.; Jiang, C.J.; Hou, Y.; Zhao, W.L.; Chen, W.; Alvarez, J.P.J. Photolysis of graphene oxide in the presence of nitrate: Implications for graphene oxide integrity in water and wastewater treatment. *Environ. Sci. Nano* **2019**, *6*, 136–145. [[CrossRef](#)]
24. Yu, F.; Huang, H.X. Simultaneously toughening and reinforcing poly(lactic acid)/thermoplastic polyurethane blend via enhancing interfacial adhesion by hydrophobic silica nanoparticles. *Polym. Test.* **2015**, *45*, 107–113. [[CrossRef](#)]
25. Yang, L.; Zhen, W.J. Poly(lactic acid)/p-phenylenediamine functionalized graphene oxidized nanocomposites: Preparation, rheological behavior and biodegradability. *Eur. Polym. J.* **2019**, *121*, 109341. [[CrossRef](#)]
26. Yang, A.W.; Li, J.J.; Zhang, C.; Zhang, W.Q.; Ma, N. One-step amine modification of graphene oxide to get a green trifunctional metal-free catalyst. *Appl. Surf. Sci.* **2015**, *346*, 443–450. [[CrossRef](#)]
27. Su, Z.; Wang, H.; Tian, K.H.; Xu, F.; Huang, W.Q.; Tian, X.Y. Simultaneous reduction and surface functionalization of graphene oxide with wrinkled structure by diethylenetriamine (DETA) and their reinforcing effects in the flexible poly(2-ethylhexyl acrylate) (P2EHA) films. *Compos. Part A Appl. Sci. Manuf.* **2016**, *84*, 64–75. [[CrossRef](#)]
28. Yu, Z.R.; Li, S.N.; Zang, J.; Zhang, M.; Gong, L.X.; Song, P.; Zhao, L.; Zhang, G.D.; Tang, L.C. Enhanced mechanical property and flame resistance of graphene oxide nanocomposite paper modified with functionalized silica nanoparticles. *Compos. Part B-Eng.* **2019**, *177*, 107347. [[CrossRef](#)]
29. Xu, B.; Maimaiti, H.; Wang, S.X.; Awati, A.; Wang, Y.; Zhang, J.H.; Chen, T.L. Preparation of coal-based graphene oxide/SiO₂ nanosheet and loading ZnO nanorod for photocatalytic Fenton-like reaction. *Appl. Surf. Sci.* **2019**, *498*, 143835. [[CrossRef](#)]
30. Li, J.; Wang, S.X.; Wang, F.; Wu, X.R.; Zhuang, X.M. Environmental separation and enrichment of gold and palladium ions by amino-modified three-dimensional graphene. *RSC Adv.* **2019**, *9*, 2816–2821. [[CrossRef](#)]
31. Ekoué, A.; Renault, O.; Billon, T.; di Cioccio, L.; Guillot, G. Study of the Wet Re-Oxidation Annealing of SiO₂/4H-SiC (0001) Interface Properties by AR-XPS Measurements. *Mater. Sci. Forum* **2003**, *433*, 555–558.
32. Yu, B.; Wang, X.; Qian, X.D.; Xing, W.Y.; Yang, H.Y.; Ma, L.Y.; Lin, Y.; Jiang, S.H.; Song, L.; Hu, Y.; et al. Functionalized graphene oxide/phosphoramidate oligomer hybrids flame retardant prepared via in situ polymerization for improving the fire safety of polypropylene. *RSC Adv.* **2014**, *4*, 31782–31794. [[CrossRef](#)]
33. Bera, M.; Gupta, P.; Maji, P.K. Efficacy of ultra-low loading of amine functionalized graphene oxide into glycidol-terminated polyurethane for high-performance composite material. *React. Funct. Polym.* **2019**, *139*, 60–74. [[CrossRef](#)]
34. Ding, G.X.; Chen, C.X.; Tai, H.X.; Tang, Z.F.; Wang, Z.F.; Cheng, G.J.; Wan, X.L. The effect of Co²⁺, Cu²⁺ element ratio on the microwave absorption properties of Co_xCu_{1-x}Fe₂O₄/RGO composites. *Mater. Lett.* **2021**, *289*, 129423. [[CrossRef](#)]
35. Gao, M.M.; Zhao, Y.; Wang, S.S.; Xu, Y.C.; Feng, C.H.; Shi, D.X.; Jiao, Q.Z. Preparation of pod-like 3D Ni_{0.33}Co_{0.67}Fe₂O₄@rGO composites and their microwave absorbing properties. *Ceram. Int.* **2019**, *45*, 7188–7195. [[CrossRef](#)]
36. Kou, L.; Gao, C. Making silica nanoparticle-covered graphene oxide nanohybrids as general building blocks for large-area superhydrophilic coatings. *Nanoscale* **2011**, *3*, 519–528. [[CrossRef](#)]
37. Wang, C.Y.; Lan, Y.F.; Yu, W.T.; Li, X.; Qian, Y.; Liu, H.S. Preparation of amino-functionalized graphene oxide/polyimide composite films with improved mechanical, thermal and hydrophobic properties. *Appl. Surf. Sci.* **2016**, *362*, 11–19. [[CrossRef](#)]
38. Wang, J.Y.; Li, Y.C.; Song, G.; Xie, Y.; Zhu, K.R.; Alsaedi, A.; Hayat, T.; Chen, C.L. Construction of novel graphene-based materials GO@SiO₂@C@Ni for Cr (VI) removal from aqueous solution. *J. Colloid Interface Sci.* **2019**, *557*, 254–265. [[CrossRef](#)]
39. Thakur, S.; Karak, N. A tough, smart elastomeric bio-based hyperbranched polyurethane nanocomposite. *New J. Chem.* **2015**, *39*, 2146–2154. [[CrossRef](#)]
40. Li, L.; Xu, L.; Ding, W.; Lu, H.Y.; Zhang, C.; Liu, T.X. Molecular-engineered hybrid carbon nanofillers for thermoplastic polyurethane nanocomposites with high mechanical strength and toughness. *Compos. Part B Eng.* **2019**, *177*, 107381. [[CrossRef](#)]
41. Ronchi, R.M.; Marchiori, C.F.N.; Araujo, C.M.; Arantes, J.T.; Santos, S.F. Thermoplastic polyurethane–Ti₃C₂(Tx) MXene nanocomposite: The influence of functional groups upon the matrix–reinforcement interaction. *Appl. Surf. Sci.* **2020**, *528*, 146526. [[CrossRef](#)]
42. Bera, M.; Maji, P.K. Effect of structural disparity of graphene-based materials on thermo-mechanical and surface properties of thermoplastic polyurethane nanocomposites. *Polymer* **2017**, *119*, 118–133. [[CrossRef](#)]
43. Qu, L.J.; Tian, M.W.; Hu, X.L.; Wang, Y.J.; Zhu, S.F.; Guo, X.Q.; Han, G.T.; Zhang, X.S.; Sun, K.K.; Tang, X.N. Functionalization of cotton fabric at low graphene nanoplate content for ultrastrong ultraviolet blocking. *Carbon* **2014**, *80*, 565–574. [[CrossRef](#)]
44. Pandey, S.; Jana, K.K.; Aswal, V.K.; Rana, D.; Maiti, P. Effect of nanoparticle on the mechanical and gas barrier properties of thermoplastic polyurethane. *Appl. Clay Sci.* **2017**, *146*, 468–474. [[CrossRef](#)]
45. Bae, G.; Ahn, C.; Jeon, S. Transparent polymer nanocomposite with three-dimensional ZnO thin-shell with high UV-shielding performance. *Funct. Compos. Struct.* **2021**, *3*, 025007. [[CrossRef](#)]
46. Gao, Q.S.; Feng, M.J.; Li, E.; Liu, C.T.; Shen, C.Y.; Liu, X.H. Mechanical, Thermal, and Rheological Properties of Ti₃C₂TxMXene/ Thermoplastic Polyurethane Nanocomposites. *Macromol. Mater. Eng.* **2020**, *305*, 2000343. [[CrossRef](#)]